Gain-dependent Purcell enhancement, breakdown of Einstein's relations, and superradiance in nanolasers

Andrey A. Vyshnevyy*

Center for Photonics and 2D Materials, Moscow Institute of Physics and Technology, Dolgoprudny, 141700, Russian Federation

(Received 18 February 2021; revised 16 December 2021; accepted 27 January 2022; published 9 February 2022)

Light emitters in a single-mode nanolaser interact with the same cavity field that gives rise to polarization correlations which transform the cavity mode. Usually these correlations are ignored, however, collective phenomena can lead to the distinct sub- and superradiance, whose fully quantum description is challenging. Here we develop a simple yet rigorous picture of radiative transitions in single-mode nanolasers that accounts for polarization correlations. We show that the collective behavior of emitters modifies the photonic density of states leading to gain-dependent Purcell enhancement of spontaneous emission. Moreover, the stimulated emission rate is dependent on both the photon number and the laser line shape. As the laser line narrows, stimulated emission becomes stronger than predicted by Einstein's relations and the nanolaser reaches the threshold earlier. Finally, we provide concise, ready-to-use expressions for spontaneous and stimulated emission rates seamlessly describing both conventional and superradiant nanolasers.

DOI: 10.1103/PhysRevB.105.085116

I. INTRODUCTION

The Purcell effect, first noted in 1946 for radio frequencies [1], has become a foundation of nanophotonics, playing a pivotal role in surface-enhanced Raman spectroscopy [2], ultrafast response dynamics of nanoscale sources of light [3], and enabling bright and efficient single-photon emitters [4,5]. The advances in fabrication technology enabled the production of nanolasers, the record small sources of coherent light [6–17], realizing collective coupling of emitters to a single subwavelength-scaled cavity. Apart from obvious practical applications, nanolasers attract research interest by their unique and rich physics, including the thresholdless lasing [10,11], delayed and gradual transition to coherent state [18,19], antibunching [20], and many other phenomena. The standard approach to nanolaser modeling employs rate equations [21,22], in which the spontaneous and stimulated emission rates originate from Fermi's golden rule [23]. However, Fermi's golden rule is initially derived for isolated discrete levels not engaged in any interaction except that with the continuum of states. In contrast, electronic states in nanolasers' gain media are disturbed by other charge carriers and phonons, causing their spectral broadening. To treat this disturbance rigorously, radiative phenomena must be studied microscopically.

Using the master equation approach, Ujihara [24] found the spontaneous emission rate of a single broadened excited emitter into the cavity mode as

$$r_{\mathrm{sp}} = \frac{2\pi |g|^2}{\hbar^2} \int \rho_{\mathrm{e}}(\omega)\rho(\omega)d\omega, \tag{1}$$

where $\rho_{\mathrm{e}}(\omega)$ and $\rho(\omega)$ are Lorentzian densities of states per unit of angular frequency for the emitter and the cavity mode, respectively, and g is the light-matter coupling constant. Gu and coauthors obtain a similar expression [25], except that their collisional dephasing model yields a non-Lorentzian density of states for emitters. To obtain the stimulated decay rate, one multiplies the spontaneous emission rate by the number of photons in the cavity N_{p}, as dictated by Einstein's relations for radiative transitions:

$$r_{\mathrm{stim}} = N_{\mathrm{p}} r_{\mathrm{sp}}. \tag{2}$$

Taking into account that only a fraction of emitters are excited by a factor $n_2(1 - n_1)$, where $n_{2(1)}$ are populations of the excited (ground) states, one usually finds the total spontaneous emission rate as:

$$R_{\mathrm{sp}} = N n_2 (1 - n_1) r_{\mathrm{sp}}, \tag{3}$$

where N is the number of emitters in the gain medium. The total stimulated emission rate combines the absorption and emission processes in a single term:

$$R_{\mathrm{stim}} = N(n_2 - n_1) r_{\mathrm{stim}}. \tag{4}$$

In the above expressions, r_{sp} and r_{stim} are defined by Eqs. (1) and (2).

The laser rate equation model incorporating Eqs. (3) and (4) (hereafter abbreviated as REM) shows good agreement with the many-body microscopic model [26] based on the cluster-expansion approach [27,28]. Although some authors consider the Purcell enhancement independently from the stimulated emission [29], REM currently embodies the established consensus [30]. However, Eqs. (1) and (2) treat each quantum emitter independently and ignore their collective behavior. All emitters interact with the same cavity mode; therefore their small individual polarizations contribute coherently to a macroscopic electric dipole moment. This dipole

*andrey.vyshnevyy@phystech.edu

moment affects the dynamics of the laser mode, which, in turn, may significantly modify the radiation rates when the cavity linewidth is comparable or larger than the emitters linewidth [25,31,32]. This effect is referred to as sub- and superradiance, depending on whether the emission is suppressed or enhanced.

The increasing interest in superradiant lasers is driven by the ability to emit very strong pulses [33], stability of the emission wavelength to fluctuations of the cavity resonance [34], and generation of superthermal light [32,33]. Furthermore, most spasers or dielectric nanolasers with highly confined open cavity modes are expected to operate in superradiant regime thanks to low quality factor of the cavity resonance.

Within the semiclassical lasing picture, collective effects are already accounted for by the semiclassical Maxwell-Bloch equations (SMBE), which, as we note below, predict lower threshold population inversion than REM. At the same time, SMBE ignore spontaneous emission into the cavity mode because they treat electromagnetic field classically.

A fully quantum description of superradiance in nanolasers is challenging. Existing methods rely on cluster expansion approach [31–33] or supplement SMBE with the Langevin forces [35,36]. The former approach can describe any experimental setting; however, it results in a cumbersome set of coupled equations that provide limited insight. The latter is mainly applicable to atomic gain media and therefore ignores the Pauli blocking effects relevant to all nanolasers with semiconductor quantum dots as the source of optical gain.

Here we provide a simple picture of radiative transitions in nanolasers, including sub- and superradiance. The theory is derived using the rigorous Keldysh formalism for nonequilibrium Green's functions. We preserve convenient "golden rulelike" expressions for the spontaneous and stimulated emission rates and show that sub- and superradiance in spontaneous emission emerges from the transformation of photonic density of states $\rho(\omega)$ caused by polaritonic transformation (dressing) of the cavity mode; $\rho(\omega)$ depends on the population inversion, thus superradiance in nanolasers can be understood as gain-dependent Purcell enhancement. On the other hand, stimulated emission is enhanced by line narrowing, hence the reduced threshold compared with REM and violation of Einstein's relations for single-mode lasers. Notably, our model shows that sub- and superradiance in nanolasers can appear even without the modification of the collective electronic state, described in the seminal work by Dicke [37].

II. NANOLASER MODEL

We consider the Tavis-Cummings model [38] for the interaction of an ensemble of two-level emitters with the single-mode quantized field in a cavity:

$$H = H_{\rm em} + H_{\rm cav} + H_{\rm int}, \tag{5}$$

where Hamiltonians of the emitters and the cavity ($\hbar = 1$) are $H_{\rm em} = \sum_{i=1}^{N}(\varepsilon_1 c_{1i}^{\dagger}c_{1i} + \varepsilon_2 c_{2i}^{\dagger}c_{2i})$ and $H_{\rm cav} = \omega_{\rm c} a^{\dagger}a$ correspondingly. Here ε_1, ε_2 are the energies of the ground and excited emitter states; $\omega_{\rm c}$ is the central frequency of the cavity mode; $c_{1i}^{(\dagger)}$, $c_{2i}^{(\dagger)}$, $a^{(\dagger)}$ are annihilation (creation) operators

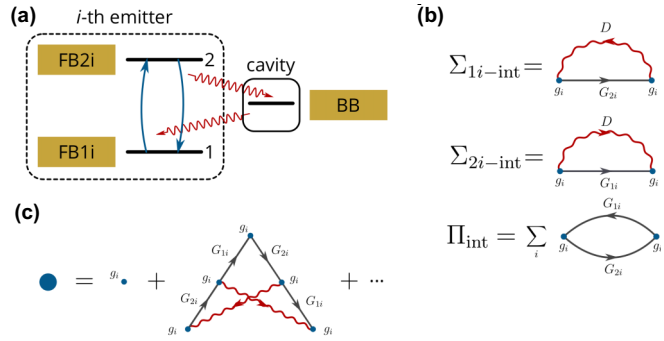

FIG. 1. (a) Schematic of the laser model comprising N two-leveled emitters radiatively coupled to the cavity mode. Ground (labeled 1) and excited (labeled 2) levels of each emitter are coupled to fermionic reservoirs (labeled FB1i and FB2i for the *ith* emitter) responsible for incoherent pumping and collection of electrons and homogeneous broadening of electronic levels. Cavity loss is modeled by coupling to bosonic bath BB. (b) Self-energies originating from light-matter interaction in the system for the cavity photons $\Pi_{\rm int}$, ground $\Sigma_{1i-\rm int}$, and excited $\Sigma_{2i-\rm int}$ electronic levels. (c) Vertex function expansion showing the leading-order correction.

of the ground and excited levels of the *ith* emitter and the cavity mode, respectively; N is the number of emitters in the cavity. Light-matter interaction is governed by $H_{\rm int} = \sum_{i=1}^{N}(g_i c_2^{\dagger}c_1 a + \text{H.c.})$, where g_i is the constant of light-matter coupling. To achieve lasing, one should pump the excited electronic state and collect electrons from the ground state, which in our model is realized by connecting each emitter's electronic levels to corresponding fermionic reservoirs, as shown in Fig. 1(a). The cavity loss is modeled as coupling to a bosonic bath. Here we do not impose restriction $c_1^{\dagger}c_1 + c_2^{\dagger}c_2 = 1$ and allow electrons to populate the excited and ground levels independently, which applies to gain media based on semiconductor quantum dots [28]. Also, the absence of the restriction allows for a more straightforward diagrammatic treatment than otherwise [39].

We study the described driven-dissipative Tavis-Cummings model using the Keldysh diagrammatic technique [40] for nonequilibrium Green's functions [41]. Within this method all observables are defined through the Green's functions of electronic and photonic states, while the emission rates follow directly from quantum kinetic equations. Importantly, we can account for large dipole moment of the gain medium in all perturbation orders via the partial summation of relevant diagrams.

Couplings to the fermionic reservoirs are described by the retarded and lesser self-energies [42] $\Sigma^{R}_{\rm FB1,2i}(\omega) = -i\gamma_{1,2}/2$ and $\Sigma^{<}_{\rm FB1,2i}(\omega) = i n^{0}_{1,2}\gamma_{1,2}$, whereas similar self-energies for the coupling to a bosonic bath are $\Pi^{R}_{\rm BB}(\omega) = -i\kappa/2$ and, neglecting thermal occupancy of the bosonic bath, $\Pi^{<}_{\rm BB}(\omega) = 0$. Here κ, γ_1, γ_2 are the photonic modes damping rate and tunneling rates to the ground and excited levels, correspondingly. Superscripts $<, >, R, A$ denote the lesser, greater, retarded, and advanced components of Green's functions and self-energies. For simplicity, we let populations $n^{0}_{1,2}$ of FB1i and FB2i be energy-independent. We focus on the steady-state

solution, thus for any quantity O: $O^A(\omega) = [O^R(\omega)]^*$. Also, $O^> = O^< + O^R - O^A$.

Figure 1(b) depicts self-energies from light-matter interaction. We treat the interaction self-consistently, which means that all lines in diagrams in Fig. 1(b) label dressed Green's functions. Our approximation is valid when the number of photons in the cavity is not too large so that the corrections to the vertex function, shown in Fig. 1(c), can be neglected. The components of interaction-induced polarization operator read

$$\Pi^R_{\rm int}(\omega) = -i\sum_{i=1}^{N}|g_i|^2\int\frac{d\omega'}{2\pi}[G^<_{1i}(\omega')G^R_{2i}(\omega'+\omega) + G^A_{1i}(\omega')G^<_{2i}(\omega+\omega')], \tag{6}$$

$$\Pi^{\lessgtr}_{\rm int}(\omega) = -i\sum_{i=1}^{N}|g_i|^2\int\frac{d\omega'}{2\pi}G^{\gtrless}_{1i}(\omega')G^{\lessgtr}_{2i}(\omega'+\omega), \tag{7}$$

where $G_{1,2i}$ denote Green's functions of the *ith* emitters electronic levels. To derive the emission rates, we use the Kadanoff-Baym (quantum rate) equations. In the stationary state,

$$0 = \frac{\partial N_{\rm p}}{\partial t} = \int\frac{d\omega}{2\pi}[\Pi^R(\omega) - \Pi^A(\omega)]D^<(\omega) + \int\frac{d\omega}{2\pi}\Pi^<(\omega)[D^A(\omega) - D^R(\omega)], \tag{8}$$

in which $N_{\rm p}$ is the number of photons and $D(\omega)$ is the Fourier transform of the photonic Green's function $D(t,t') = -i\langle\mathcal{T}_K[a(t)a^\dagger(t')]\rangle$, where $\mathcal{T}_K$ denotes time ordering along the Keldysh contour. The polarization operator contains both the dissipative and the interaction parts $\Pi = \Pi_{\rm BB} + \Pi_{\rm int}$. In this rate equation, the total stimulated and spontaneous emission rates into the cavity mode are given by

$$R^{\rm tot}_{\rm stim} = \int\frac{d\omega}{2\pi}\left[\Pi^R_{\rm int}(\omega) - \Pi^A_{\rm int}(\omega)\right]D^<(\omega), \tag{9}$$

$$R^{\rm tot}_{\rm sp} = \int\frac{d\omega}{2\pi}\Pi^<_{\rm int}(\omega)[D^A(\omega) - D^R(\omega)]. \tag{10}$$

The physical meaning of these equations becomes clear after we introduce photonic $\rho(\omega) = (-1/\pi){\rm Im}[D^R(\omega)]$ and electronic $\rho_{1,2i}(\omega) = (-1/\pi){\rm Im}[G^R_{1,2i}(\omega)]$ spectral functions (densities of states) and corresponding nonequilibrium populations $n(\omega)$ and $n_{1,2i}(\omega)$: $D^<(\omega) = -2\pi i n(\omega)\rho(\omega)$, $G^<_{1,2i}(\omega) = 2\pi i n_{1,2i}(\omega)\rho_{1,2i}(\omega)$. Using the identity $\Pi^R - \Pi^A = \Pi^> - \Pi^<$, we express the spontaneous and stimulated emission rates of the *ith* emitter as

$$r_{\rm i-sp} = 2\pi|g_i|^2\int d\omega d\omega' n_{2i}(\omega+\omega')[1 - n_{1i}(\omega')] \times \rho_2(\omega+\omega')\rho_1(\omega')\rho(\omega), \tag{11}$$

$$r_{\rm i-stim} = 2\pi|g_i|^2\int d\omega d\omega'[n_{2i}(\omega+\omega') - n_{1i}(\omega')] \times \rho_2(\omega+\omega')\rho_1(\omega')n(\omega)\rho(\omega). \tag{12}$$

The obtained equations are very similar to those for the rates of interband transitions in bulk semiconductors [23]. Note that Eqs. (11) and (12) treat initially discrete bound electronic levels and the cavity mode as if they are energy bands with energy-dependent populations and densities of states. Transformation of the discrete level into an energy band can be qualitatively explained by its interaction with the continuum of reservoir modes, producing a continuum of hybridized "modes of the Universe" with different coupling strengths to the quantum emitter. Energy-dependent populations and densities of states absorb non-Markovian many-body effects into convenient "golden-rule-like" form. Pumping and dephasing, as well as radiative transitions themselves, self-consistently determine the densities of states and population functions. The nonequilibrium photonic population is dictated by the balance of the *spectral densities* of emission and loss rates in Eq. (8), leading to

$$n(\omega) = \Pi^</(\Pi^R - \Pi^A). \tag{13}$$

Finally, the retarded Green's function required for the calculation of the photonic density of states is given by the Schwinger-Dyson equation

$$[D^R(\omega)]^{-1} = \omega - \omega_{\rm c} - \Pi^R(\omega). \tag{14}$$

Similar equations determine the densities of states of electronic levels $\rho_1(\omega)$, $\rho_2(\omega)$ and their frequency-dependent populations $n_1(\omega)$, $n_2(\omega)$. In addition to the transformation of the cavity mode, the full set of self-consistent equations describes a nonlinear optical response of the gain medium which includes population-related phenomena, such as gain saturation and spectral hole burning, and mixing of electronic levels via the strong cavity field usually named the AC Stark effect. For the sake of simplicity, we first focus on the transformation of the cavity mode while neglecting nonlinearities in the gain medium.

III. NANOLASER IN THE LIMIT OF A LINEAR GAIN MEDIUM

We assume that all coupling constants are equal $g_i = g$ and ignore the transformations of the emitters levels and densities of states by the cavity field. Mathematically this corresponds to the limit of $g \to 0$, $N \to \infty$ while $|g|^2N$ is constant. Such a limit matches SMBE [43]. For any finite number of photons in the cavity, we can ignore the contributions from light-matter interaction to total self-energies of the electronic states $\Sigma_{1,2i} \approx \Sigma_{\rm FB1,2i}$ and, more importantly, vertex corrections [Fig. 1(c)]. As a result, the electronic densities of states are the usual Lorentzian functions

$$\rho_{1,2}(\omega) = \frac{\gamma_{1,2}/(2\pi)}{(\omega - \varepsilon_{1,2})^2 + (\gamma_{1,2}/2)^2}, \tag{15}$$

while the populations of electronic levels coincide with those of the fermionic reservoirs $n_{1,2}(\omega) = n^0_{1,2}$. However, we should account for the interaction in polarization operator $\Pi = \Pi_{\rm BB} + \Pi_{\rm int}$. Using Eq. (6), we find the retarded interaction-induced polarization operator responsible for the polaritonic transformation of the cavity mode,

$$\Pi^R_{\rm int}(\omega) = -\frac{|g|^2N(n^0_2 - n^0_1)}{\omega - \omega_{21} + i\gamma_{\rm e}/2}, \tag{16}$$

where $\omega_{21} = \varepsilon_2 - \varepsilon_1$ and $\gamma_e = \gamma_1 + \gamma_2$. Light-matter interaction produces a term that is proportional to the classical electric susceptibility of the gain medium. The retarded Green's function, evaluated from Eq. (14), gives the photonic density of states modified by the gain medium,

$$\rho(\omega) = -\frac{1}{\pi}\mathrm{Im}\left[\omega - \omega_c + i\frac{\kappa}{2} + \frac{|g|^2 N\left(n_2^0 - n_1^0\right)}{\omega - \omega_{21} + i\gamma_e/2}\right]^{-1} \quad (17)$$

It is worth noting that, within the studied limit, the photonic Green's function is the Green's function of SMBE:

$$\begin{aligned} id_t D^R &= (\omega_c - i\kappa/2)D^R + g^* P + \delta(t), \\ id_t P &= (\omega_{21} - i\gamma_e/2)P + gD^R N\left(n_2^0 - n_1^0\right), \end{aligned} \quad (18)$$

where P denotes the dipole moment of gain medium.

Next, instead of the photonic population, we directly extract the line shape function $S(\omega) = n(\omega)\rho(\omega)$ by balancing photon emission and loss, which gives

$$\kappa S(\omega) = R_{sp}(\omega) + \mathcal{G}(\omega)S(\omega), \quad (19)$$

where $R_{sp}(\omega) = 2\pi N|g|^2 n_2^0(1 - n_1^0)\rho_e(\omega)\rho(\omega)$ is the rate of spontaneous emission of all emitters per unit of angular frequency, and $\mathcal{G}(\omega) = 2\pi N|g|^2(n_2^0 - n_1^0)\rho_e(\omega)$ is the modal gain spectrum, with $\rho_e(\omega) = \int d\omega' \rho_1(\omega')\rho_2(\omega + \omega')$ being the emitter's density of states. Once $S(\omega)$ is determined, we can calculate the spontaneous and stimulated emission rates as

$$R_{sp}^{tot} = \int R_{sp}(\omega)d\omega, \quad R_{stim}^{tot} = \int \mathcal{G}(\omega)S(\omega)d\omega. \quad (20)$$

These equations are very similar to Eqs. (3) and (4). In fact, one can recover Eqs. (3) and (4) from Eq. (20) by manually setting up

$$\rho(\omega) = \frac{\kappa/(2\pi)}{(\omega - \omega_c)^2 + (\kappa/2)^2} \quad (21)$$

and $S(\omega) = N_p\rho(\omega)$. This means that observable characteristics of lasing, such as line narrowing and frequency pulling, are the result of the cavity mode transformation under the collective dipole moment of emitters. Importantly, this transformation occurs in any structure capable of lasing, regardless of the number of emitters and the coupling strength between the emitters and the cavity mode. Thus fundamentally, lasers always operate beyond the weak coupling regime.

To determine the laser threshold, we analyze the poles of $D^R(\omega)$ shown in Fig. 2(a). They obey the equation

$$(\omega - \omega_c + i\kappa/2)(\omega - \omega_{21} + i\gamma_e/2) + |g|^2 N\left(n_2^0 - n_1^0\right) = 0, \quad (22)$$

solving which we find that one of the poles crosses the real axis at $\omega_0 = \omega_c + \kappa\Delta/(\kappa + \gamma_e)$ when $\mathcal{G}(\omega_0) = \kappa$, or, in terms of the population inversion, when

$$n_2^0 - n_1^0 = \frac{\gamma_e\kappa}{4N|g|^2}\left[1 + \left(\frac{2\Delta}{\kappa + \gamma_e}\right)^2\right]. \quad (23)$$

Above, $\Delta = \omega_{21} - \omega_c$ is the detuning between the emitters and the cavity. Notably, our nanolaser model predicts a different lasing threshold from REM. The latter reaches the balance between stimulated emission and the photon loss $2\pi N|g|^2(n_2^0 - n_1^0)N_p\int \rho_e(\omega)\rho(\omega)d\omega = \kappa N_p$ at a population inversion of

$$n_2^0 - n_1^0 = \frac{(\gamma_e + \kappa)\kappa}{4N|g|^2}\left[1 + \left(\frac{2\Delta}{\kappa + \gamma_e}\right)^2\right], \quad (24)$$

exceeding the value in Eq. (23) by a factor of $(\gamma_e + \kappa)/\gamma_e$. At the same time, Eq. (23) agrees with SMBE, while the threshold of REM is not [43]. Unlike REM, SMBE include the collective dipole moment of emitters classically, thus the obtained agreement can be understood as a particular case of quantum-classical correspondence.

Figures 2(b) and 2(c) show how the optical density of states and the line shape function evolve with the increase in

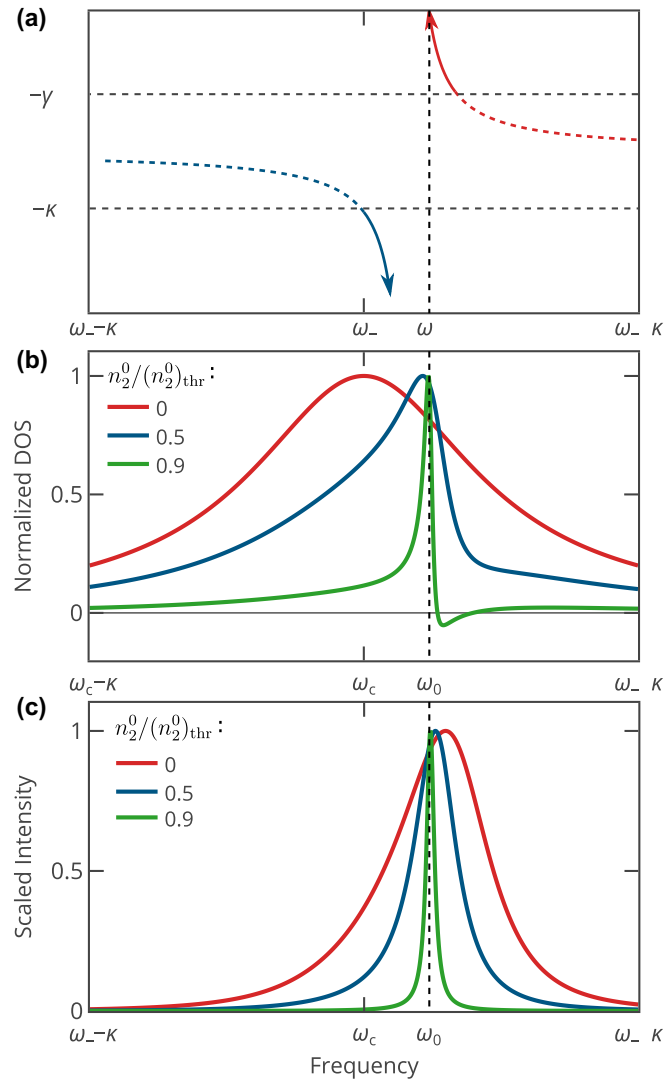

FIG. 2. (a) Poles of the retarded photonic Green's function as a function of population inversion. Arrows show the direction of increase in inversion. Dashed parts of the curves are relevant to negative inversion $n_2^0 < n_1^0$, i.e., absorbing gain medium. (b) The optical density of states $\rho(\omega)$ normalized to its maximum value and (c) the normalized emission spectrum plotted at different degrees of population inversion. All calculations assume $\Delta = \kappa/3$, $\gamma_e = 0.4\kappa$, $n_1^0 = 0$; $(n_2^0)_{thr}$ denotes the threshold population of the excited level given by Eq. (23).

population inversion. For illustrative purposes, we assumed $\Delta = \kappa/3$, $\gamma_e = 0.4\kappa$, $n_1^0 = 0$. Remarkably, the optical density of states is negative in a limited spectral band corresponding to $\mathcal{G}(\omega) > \kappa$. Although negative densities of states look exotic and are impossible in purely lossy environments, they have been reported for optical systems which combine amplifying and absorptive media [44]. At the same time, no exotic behavior is seen in the calculated line shape function $S(\omega)$ which remains positively valued and exhibits peak narrowing and frequency pulling. As the population inversion approaches its threshold value, the laser luminescence peak approaches ω_0, which again fully agrees with SMBE [43].

Although the photonic density of states and the line shape function have complicated profiles, it is possible to calculate the total spontaneous and stimulated emission rates analytically. After some algebra exploiting the residue theorem (see Supplement 1, Sections I and II for details in the Supplemental Material [45]), we obtain one of key results of this paper:

$$R_{sp}^{tot} = n_2^0\left(1 - n_1^0\right)\frac{N|g|^2}{\hbar^2}\frac{\kappa + \gamma_e - \mathcal{G}_{max}/2}{\Delta^2 + \left(\frac{\kappa+\gamma_e-\mathcal{G}_{max}/2}{2}\right)^2}, \quad (25)$$

$$R_{stim}^{tot} = \kappa N_p - R_{sp}^{tot}, \quad (26)$$

where the number of photons in the cavity is

$$N_p = \int S(\omega)d\omega = \frac{\frac{4N|g|^2}{\hbar^2}\frac{n_2^0(1-n_1^0)}{\kappa+\gamma_e}}{\kappa\left[1 + \left(\frac{2\Delta}{\kappa+\gamma_e}\right)^2\right] - \mathcal{G}_{max}}, \quad (27)$$

and $\mathcal{G}_{max} = \mathcal{G}(\omega_{21}) = 4N(|g|^2/\hbar^2)(n_2^0 - n_1^0)/\gamma_e$. In the above expressions we have restored $\hbar$ for the convenience.

The effect of the polaritonic transformation on the total spontaneous emission rate is equivalent to the reduction of the effective cavity damping rate. As a result, Eq. (25) predicts the increase in the total spontaneous emission rate, i.e., superradiance, at positive population inversion ($G_{max} > 0$) and subradiance when the gain medium absorbs light ($G_{max} < 0$), unless Δ is very large. This leads to gain-dependent values of beta and Purcell factors even in the absence of inhomogeneous broadening. In the case when $\Delta = 0$, the Purcell factor increases by a factor of 2 as the population inversion approaches the threshold value. Rates of the spontaneous and stimulated emission of radiation are connected by the Einstein relations, which in the case of a single cavity mode is typically expressed by Eq. (2). However, in our case, Eq. (2) holds only for *spectral densities* of the spontaneous and stimulated emission rates of an excited emitter $r_{stim}(\omega) = r_{sp}(\omega)n(\omega)$, while the total rates violate it due to nonuniform $n(\omega)$, as seen from Eqs. (25) and (26).

To demonstrate violation of the Einstein's relations, we plot the violation factor defined as

$$F_V = \frac{R_{stim}}{N_p R_{sp}}\frac{n_2^0 - n_1^0}{n_2^0\left(1 - n_1^0\right)} \quad (28)$$

as a function of the photon number (Fig. 3). According to this definition, $F_V = 1$ for emission rates given by Eqs. (3) and (4) which obey Einstein's relation. By contrast, the violation factor calculated using Eqs. (25) and (26) reaches above 2.75. Note, that, even when $N_p \sim 0$, i.e., when the photonic density of states is still Lorentzian, the F_V is still above 2.5, thanks to nonuniform $n(\omega)$.

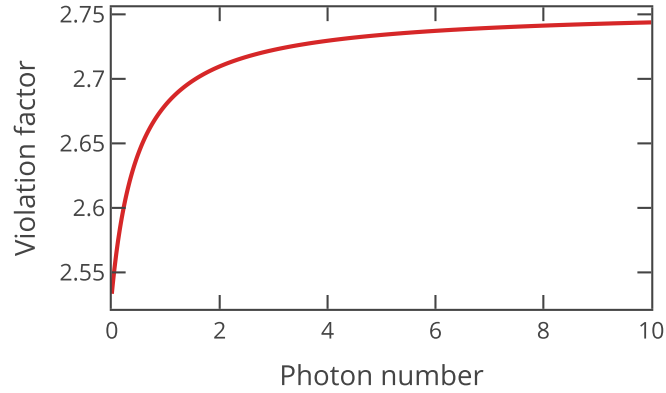

FIG. 3. Einstein's relation violation factor determined by Eq. (28) as a function of the photon number in the laser mode. The nanolaser parameters are the same as in Fig. 2.

Although our equations predict the violation of Einstein's relations, this violation becomes weak if $\kappa \ll \gamma_e$, or the nanolaser belongs to "class-B" lasers [46]. This is not the result of weak coupling but rather is caused by insensitivity of emission rates to the transformations of $\rho(\omega)$ and $S(\omega)$. In fact, one can simply assume $\rho(\omega) = \delta(\omega - \omega_c)$ and $S(\omega) = N_p\delta(\omega - \omega_c)$. At the same time, solid-state nanolasers can disobey $\kappa \ll \gamma_e$ since the quality factor of wavelength-scaled nanocavities can be as small as a few hundred [7] or even less for open cavities while γ_e of quantum dots can be made as small as 10 μeV at low temperature [47]. In such case, they are often referred to as superradiant, with a number having been experimentally realized [48,49].

IV. FEEDBACK, LASING THRESHOLD, AND LIMITATIONS OF THE THEORY

In this section, we briefly discuss the role of the cavity feedback on electronic levels and limitations of the described theory. As the population inversion increases, the number of photons in the cavity grows, eventually making light-matter-interaction-related contributions Σ_{1i-int}, Σ_{2i-int} to the electronic self-energies large. To estimate the photon number, when we can no longer neglect these contributions, we directly calculate Σ_{1i-int}^R. Assuming $N_p \gg 1$, the line shape can be approximated as $S(\omega) = N_p\delta(\omega - \omega_0)$, or, equivalently, $D^<(\omega) = -2\pi i N_p\delta(\omega - \omega_0)$. Neglecting a small contribution from $D^R(\omega)$ we find

$$\Sigma_{1i-int}^R \approx i|g|^2\int D^<(\omega')G_{2i}^R(\omega + \omega')\frac{d\omega'}{2\pi}$$

$$\approx \frac{|g|^2 N_p}{\omega + \omega_0 - \varepsilon_2 + i\gamma_2/2}. \quad (29)$$

Demanding $|\Sigma_{1i-int}^R(\omega)| \ll |\Sigma_{FB1i}^R(\omega)|$ for real frequencies, we obtain $N_p \ll \gamma_1\gamma_2/(4|g|^2)$. When the number of photons approaches this limit, two phenomena occur. First, due to the rapid stimulated emission, populations of electronic levels $n_1(\omega)$, $n_2(\omega)$ start to deviate from fermionic baths occupancies n_1^0, n_2^0, which results in gain saturation and spectral hole

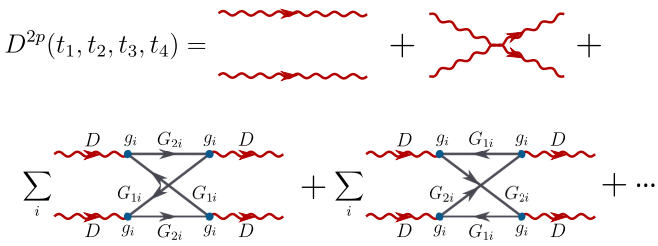

FIG. 4. Diagrammatic series for the two-particle Green's function for photons.

burning. Second, the corrections to the electronic densities of states make the modal gain spectrum $\mathcal{G}(\omega) = 2\pi N|g|^2(n_2 - n_1)\rho_e(\omega)$ explicitly dependent on the number of photons in the cavity mode, even if n_1 and n_2 are maintained at a constant level. This regime corresponds to the onset of the AC Stark effect [50]. In most nanolasers, only a small fraction of emitters homogeneous broadening is caused by the pumping or decay, with the rest of it being due to elastic phase breaking processes, thus gain saturation occurs much earlier than the AC Stark effect. In this case, $n^0_{1(2)}$ in Eqs. (25) and (27) are to be replaced with $n_{1(2)} = \langle c^\dagger_{1(2)} c_{1(2)}\rangle$, which should be obtained from $n_{1(2)} = n^0_{1(2)} \pm \kappa N_p/(N\gamma_{r1(r2)})$, where "+" corresponds to the equation for n_1, while $\gamma_{r1(r2)}$ are population relaxation rates, now different from electronic level homogeneous broadenings $\gamma_{1(2)}$.

Next, we demonstrate that our theory describes nanolasers in both the lasing and the nonlasing regimes by estimating the lasing threshold and showing that it is within limits of applicability of the developed theory. The concept of lasing and in particular lasing threshold has been attracting much attention in recent years. With the experimental demonstration of so-called thresholdless nanolasers [10], the usual definition based on features of input-output (light-light or light-current) characteristics becomes ill-defined [51]. As a result, alternative definitions have been proposed [18–20,52], most of which are based on the statistics of radiation, which is Poissonian for coherent light, while that of incoherent, or thermal, light is described by the Bose-Einstein distribution. We consider a two-particle photonic Green's function $D^{2p}(t_1,t_2,t_3,t_4) = -\langle \mathcal{T}_K[a(t_1)a(t_2)a^\dagger(t_3)a^\dagger(t_4)]\rangle$. This function is directly related to the second-order coherence function $g^{(2)}(\tau) = \frac{\langle a^\dagger(t)a^\dagger(t+\tau)a(t+\tau)a(t)\rangle}{\langle a^\dagger(t)a(t)\rangle\langle a^\dagger(t+\tau)a(t+\tau)\rangle}$, which is capable of unambiguous distinction between thermal ($g^{(2)}(0) = 2$) and coherent ($g^{(2)}(0) = 1$) radiation. Figure 4 shows the diagrammatic series for D^{2p}. The first two terms correspond to

$$\begin{aligned}&\langle a^\dagger(t)a^\dagger(t+\tau)a(t+\tau)a(t)\rangle\\ &\quad\approx \langle a^\dagger(t)a(t)\rangle\langle a^\dagger(t+\tau)a(t+\tau)\rangle\\ &\qquad+\langle a^\dagger(t)a(t+\tau)\rangle\langle a^\dagger(t+\tau)a(t)\rangle,\end{aligned} \tag{30}$$

which translates into the Siegert relation [53] $g^{(2)}(\tau) = 1 + |g^{(1)}(\tau)|^2$, where $g^{(1)}(\tau)$ is the first-order coherence function. Radiation obeying the Siegert relation is obviously thermal ($g^{(2)}(0) = 2$) since $g^{(1)}(\tau = 0) = 1$ for a single-mode electromagnetic radiation. The breakdown of the Siegert relation happens when the third and fourth terms of the diagrammatic series become comparable to the first two; that is,

$$\frac{|g|^4 N N_p^4}{\gamma_1\gamma_2\gamma_e\gamma_{line}} \sim N_p^2, \tag{31}$$

where $\gamma_{line} \ll \gamma_e$ is the FWHM of the laser peak (see Supplement 1, Section III in the Supplemental Material [45] for more details).

To determine the limits of applicability of the employed self-consistent second-order approximation we roughly estimate the previously discarded vertex correction [Fig. 1(c)]. Its relative value in the leading order does not exceed $|\delta g/g| \sim [4|g|^2 N_p/(\gamma_1\gamma_2)]^2$, setting up the limitation on the photon number $N_p \ll \gamma_1\gamma_2/(4|g|^2)$ (see Supplement 1, Section IV in the Supplemental Material [45]). When the number of photons is moderately high, the vertex correction can still be neglected compared with the corrections to the electronic Green's functions since the former is proportional to the second power of small parameter $4|g|^2 N_p/(\gamma_1\gamma_2)$ while the latter is proportional to the first power of this parameter. Notably, the photon number at the coherence threshold, determined by Eq. (31), is well within this limit; thus the developed theory applies both to nonlasing and to lasing regimes. Eventually, when $4|g|^2 N_p/(\gamma_1\gamma_2) \sim 1$, the nanolaser enters mostly unexplored regime as SMBE, REM and this theory no longer describe the physics of the nanolaser, even if $\kappa \ll \gamma_e$.

V. CONCLUSION

To summarize, we present a systematic study of lasing nanocavities with continuously pumped gain medium using the Keldysh formalism for nonequilibrium Green's functions. Our theory incorporates non-Markovian cavity-emitter dynamics and the polarization correlations between emitters into population functions and densities of states [see Eqs. (11) and (12)]. We show that nanolasers always operate beyond the weak coupling limit, as the photonic mode is transformed by the collective electric dipole moment of the emitters in the active region, which leads to sub- and superradiance. Remarkably, the discovered mechanism of sub- and superradiance is fundamentally different from the Dicke superradiance since no transformation of the electronic state is involved. Key equations of our theory (19, 20) have a simple rate equation structure. Our approach systematically adds spontaneous emission to SMBE. The use of the Keldysh formalism allowed us to maintain a sufficient level of mathematical rigor by revealing the limits of validity for all involved approximations and the error scales associated with them.

Remarkably, while the derivation relies on the Keldysh formalism, the application of the developed theory to nanolasers at $N_p \ll \gamma_1\gamma_2/(4|g|^2)$ does not require mastery of many-body perturbation theory. The retarded Green's function of photons, which describes the transformation of the photonic density of states, can be obtained directly from SMBE (18) or classical electrodynamics. The laser line shape naturally emerges from the rate equation (19). Computations of input-output curves would benefit from compact ready-to-use expressions (25, 26, 27) connecting the population inversion to the number of photons and radiative emission rates. These expressions shed light on nanolaser physics by revealing gain-dependent Purcell enhancement and breakdown of Einstein's relations due to line narrowing. Also, we predict the negative spectral

density of spontaneous emission near the lasing threshold. Finally, we discuss the nonlinear optical response of the gain medium and show that the transition to coherent emission happens within the validity limits of our theory.

With foreseeable extensions to broadband gain media, such as bulk semiconductors and quantum wells, our theory creates a firm ground for studies of many-body phenomena in active nanophotonic devices.

ACKNOWLEDGMENTS

The author was supported by the stipend of the President of the Russian Federation (SP-1125.2021.5), the Ministry of Science and Higher Education of the Russian Federation (Agreement No. 075-15-2021-606). The author is grateful to Alex Krasnok, Sergey Lepeshov, Denis Baranov and Igor Khramtsov for stimulating discussions.

[1] E. M. Purcell, Spontaneous emission probabilities at radio frequencies, Phys. Rev. **69**, 681 (1946).

[2] S. I. Maslovski and C. R. Simovski, Purcell factor and local intensity enhancement in surface-enhanced raman scattering, Nanophotonics **8**, 429 (2019).

[3] T. Suhr, N. Gregersen, K. Yvind, and J. Mørk, Modulation response of nanoLEDs and nanolasers exploiting purcell enhanced spontaneous emission, Opt. Express **18**, 11230 (2010).

[4] A. J. Bennett, D. C. Unitt, P. See, A. J. Shields, P. Atkinson, K. Cooper, and D. A. Ritchie, Microcavity single-photon-emitting diode, Appl. Phys. Lett. **86**, 181102 (2005).

[5] I. A. Khramtsov, A. A. Vyshnevyy, and D. Y. Fedyanin, Enhancing the brightness of electrically driven single-photon sources using color centers in silicon carbide, npj Quantum Inf. **4**, 15 (2018).

[6] M. T. Hill, Y.-S. Oei, B. Smalbrugge, Y. Zhu, T. de Vries, P. J. van Veldhoven, F. W. M. van Otten, T. J. Eijkemans, J. P. Turkiewicz, H. de Waardt, E. J. Geluk, S.-H. Kwon, Y.-H. Lee, R. Nötzel, and M. K. Smit, Lasing in metallic-coated nanocavities, Nat. Photonics **1**, 589 (2007).

[7] K. Ding and C. Z. Ning, Metallic subwavelength-cavity semiconductor nanolasers, Light: Sci. Appl. **1**, e20 (2012).

[8] K. Ding, M. T. Hill, Z. C. Liu, L. J. Yin, P. J. van Veldhoven, and C. Z. Ning, Record performance of electrical injection sub-wavelength metallic-cavity semiconductor lasers at room temperature, Opt. Express **21**, 4728 (2013).

[9] M. P. Nezhad, A. Simic, O. Bondarenko, B. Slutsky, A. Mizrahi, L. Feng, V. Lomakin, and Y. Fainman, Room-temperature subwavelength metallo-dielectric lasers, Nat. Photonics **4**, 395 (2010).

[10] M. Khajavikhan, A. Simic, M. Katz, J. H. Lee, B. Slutsky, A. Mizrahi, V. Lomakin, and Y. Fainman, Thresholdless nanoscale coaxial lasers, Nature (London) **482**, 204 (2012).

[11] I. Prieto, J. M. Llorens, L. E. Muñoz-Camúñez, A. G. Taboada, J. Canet-Ferrer, J. M. Ripalda, C. Robles, G. Muñoz-Matutano, J. P. Martínez-Pastor, and P. A. Postigo, Near thresholdless laser operation at room temperature, Optica **2**, 66 (2015).

[12] S. Wu, S. Buckley, J. R. Schaibley, L. Feng, J. Yan, D. G. Mandrus, F. Hatami, W. Yao, J. Vučković, A. Majumdar *et al.*, Monolayer semiconductor nanocavity lasers with ultralow thresholds, Nature (London) **520**, 69 (2015).

[13] J. S. T. Gongora, A. E. Miroshnichenko, Y. S. Kivshar, and A. Fratalocchi, Anapole nanolasers for mode-locking and ultrafast pulse generation, Nat. Commun. **8**, 15535 (2017).

[14] D. Y. Fedyanin, A. V. Krasavin, A. V. Arsenin, and A. V. Zayats, Lasing at the nanoscale: coherent emission of surface plasmons by an electrically driven nanolaser, Nanophotonics **9**, 3965 (2020).

[15] E. Tiguntseva, K. Koshelev, A. Furasova, P. Tonkaev, V. Mikhailovskii, E. V. Ushakova, D. G. Baranov, T. Shegai, A. A. Zakhidov, Y. Kivshar *et al.*, Room-temperature lasing from Mie-resonant nonplasmonic nanoparticles, ACS Nano **14**, 8149 (2020).

[16] W. Du, C. Li, J. Sun, H. Xu, P. Yu, A. Ren, J. Wu, and Z. Wang, Nanolasers based on 2D materials, Laser Photonics Rev. **14**, 2000271 (2020).

[17] A. S. Polushkin, E. Y. Tiguntseva, A. P. Pushkarev, and S. V. Makarov, Single-particle perovskite lasers: From material properties to cavity design, Nanophotonics **9**, 599 (2020).

[18] A. A. Vyshnevyy and D. Y. Fedyanin, Lasing threshold of thresholdless and non-thresholdless metal-semiconductor nanolasers, Opt. Express **26**, 33473 (2018).

[19] F. Lohof, R. Barzel, P. Gartner, and C. Gies, Delayed Transition to Coherent Emission in Nanolasers with Extended Gain Media, Phys. Rev. Appl. **10**, 054055 (2018).

[20] W. W. Chow, F. Jahnke, and C. Gies, Emission properties of nanolasers during the transition to lasing, Light: Sci. Appl. **3**, e201 (2014).

[21] H. Yokoyama and S. D. Brorson, Rate equation analysis of microcavity lasers, J. Appl. Phys. **66**, 4801 (1989).

[22] G. Bjork and Y. Yamamoto, Analysis of semiconductor microcavity lasers using rate equations, IEEE J. Quantum Electron. **27**, 2386 (1991).

[23] H. C. Casey, Jr. and M. B. Panish, *Heterostructure Lasers, Part A: Fundamental Principles* (Academic Press, New York, 1978).

[24] K. Ujihara, Spontaneous emission in a micro optical cavity from spectrally broadened atoms, Opt. Commun. **103**, 265 (1993).

[25] Q. Gu, B. Slutsky, F. Vallini, J. S. T. Smalley, M. P. Nezhad, N. C. Frateschi, and Y. Fainman, Purcell effect in sub-wavelength semiconductor lasers, Opt. Express **21**, 15603 (2013).

[26] M. Lorke, T. Suhr, N. Gregersen, and J. Mørk, Theory of nanolaser devices: Rate equation analysis versus microscopic theory, Phys. Rev. B **87**, 205310 (2013).

[27] J. Fricke, Transport equations including many-particle correlations for an arbitrary quantum system: A general formalism, Ann. Phys. **252**, 479 (1996).

[28] C. Gies, J. Wiersig, M. Lorke, and F. Jahnke, Semiconductor model for quantum-dot-based microcavity lasers, Phys. Rev. A **75**, 013803 (2007).

[29] E. K. Lau, A. Lakhani, R. S. Tucker, and M. C. Wu, Enhanced modulation bandwidth of nanocavity light emitting devices, Opt. Express **17**, 7790 (2009).

[30] B. Romeira and A. Fiore, Purcell effect in the stimulated and spontaneous emission rates of nanoscale semiconductor lasers, IEEE J. Quantum Electron. **54**, 2000412 (2018).

[31] H. A. M. Leymann, A. Foerster, F. Jahnke, J. Wiersig, and C. Gies, Sub- and Superradiance in Nanolasers, Phys. Rev. Appl. **4**, 044018 (2015).

[32] S. Kreinberg, W. W. Chow, J. Wolters, C. Schneider, C. Gies, F. Jahnke, S. Höfling, M. Kamp, and S. Reitzenstein, Emission from quantum-dot high-β microcavities: Transition from spontaneous emission to lasing and the effects of superradiant emitter coupling, Light: Sci. Appl. **6**, e17030 (2017).

[33] F. Jahnke, C. Gies, M. Aßmann, M. Bayer, H. A. M. Leymann, A. Foerster, J. Wiersig, C. Schneider, M. Kamp, and S. Höfling, Giant photon bunching, superradiant pulse emission and excitation trapping in quantum-dot nanolasers, Nat. Commun. **7**, 11540 (2016).

[34] J. G. Bohnet, Z. Chen, J. M. Weiner, D. Meiser, M. J. Holland, and J. K. Thompson, A steady-state superradiant laser with less than one intracavity photon, Nature (London) **484**, 78 (2012).

[35] E. C. André, I. E. Protsenko, A. V. Uskov, J. Mørk, and M. Wubs, On collective Rabi splitting in nanolasers and nano-LEDs, Opt. Lett. **44**, 1415 (2019).

[36] I. E. Protsenko, A. V. Uskov, E. C. André, J. Mørk, and M. Wubs, Quantum Langevin approach for superradiant nanolasers, New J. Phys. **23**, 063010 (2021).

[37] R. H. Dicke, Coherence in spontaneous radiation processes, Phys. Rev. **93**, 99 (1954).

[38] M. Tavis and F. W. Cummings, Exact solution for an N-molecule—radiation-field Hamiltonian, Phys. Rev. **170**, 379 (1968).

[39] Y. Shchadilova, M. M. Roses, E. G. Dalla Torre, M. D. Lukin, and E. Demler, Fermionic formalism for driven-dissipative multilevel systems, Phys. Rev. A **101**, 013817 (2020).

[40] L. V. Keldysh, Diagram technique for nonequilibrium processes, Zh. Eksp. Teor. Fiz. **47**, 1515 (1964) [Sov. Phys. JETP **20**, 1018 (1965)].

[41] G. Stefanucci and R. van Leeuwen, *Nonequilibrium Many-Body Theory of Quantum Systems: A Modern Introduction* (Cambridge University Press, Cambridge, 2013).

[42] P. I. Arseev, On the nonequilibrium diagram technique: derivation, some features, and applications, Phys. Usp. **58**, 1159 (2015).

[43] L. Narducci and N. Abraham, *Laser Physics and Laser Instabilities* (World Scientific, Singapore, 1988).

[44] S. Franke, J. Ren, M. Richter, A. Knorr, and S. Hughes, Fermi's Golderule for Spontaneous Emission in Absorptive and Amplifying Media, Phys. Rev. Lett. **127**, 013602 (2021).

[45] See Supplemental Material at http://link.aps.org/supplemental/10.1103/PhysRevB.105.085116 for a detailed derivation of Eqs. (25) and (27) and an estimation of the two-particle photonic Green's function and vertex correction.

[46] F. Arecchi, G. Lippi, G. Puccioni, and J. Tredicce, Deterministic chaos in laser with injected signal, Opt. Commun. **51**, 308 (1984).

[47] A. V. Kuhlmann, J. H. Prechtel, J. Houel, A. Ludwig, D. Reuter, A. D. Wieck, and R. J. Warburton, Transform-limited single photons from a single quantum dot, Nat. Commun. **6**, 8204 (2015).

[48] M. Lermer, N. Gregersen, M. Lorke, E. Schild, P. Gold, J. Mørk, C. Schneider, A. Forchel, S. Reitzenstein, S. Höfling *et al.*, High beta lasing in micropillar cavities with adiabatic layer design, Appl. Phys. Lett. **102**, 052114 (2013).

[49] M. Aßmann, F. Veit, M. Bayer, C. Gies, F. Jahnke, S. Reitzenstein, S. Höfling, L. Worschech, and A. Forchel, Ultrafast tracking of second-order photon correlations in the emission of quantum-dot microresonator lasers, Phys. Rev. B **81**, 165314 (2010).

[50] X. Xu, B. Sun, E. D. Kim, K. Smirl, P. R. Berman, D. G. Steel, A. S. Bracker, D. Gammon, and L. J. Sham, Single Charged Quantum Dot in a Strong Optical Field: Absorption, Gain, and the ac-Stark Effect, Phys. Rev. Lett. **101**, 227401 (2008).

[51] C.-Z. Ning, What is laser threshold? IEEE J. Sel. Top. Quantum Electron. **19**, 1503604 (2013).

[52] A. A. Vyshnevyy and D. Y. Fedyanin, Elusive coherence of metal-semiconductor nanolasers, in *Conference on Lasers and Electro-Optics, OSA Technical Digest, Washington, DC* (Optical Society of America, 2020), paper SF1E.5.

[53] A. Siegert, *On the Fluctuations in Signals Returned by Many Independently Moving Scatterers* (Radiation Laboratory, Massachusetts Institute of Technology, Cambridge, MA, 1943).